

# Strange metal behavior in a pure ferromagnetic Kondo lattice

Bin Shen,<sup>1,\*</sup> Yongjun Zhang,<sup>1,\*</sup> Yashar Komijani,<sup>2,\*</sup> Michael Nicklas,<sup>3</sup> Robert Borth,<sup>3</sup> An Wang,<sup>1</sup> Ye Chen,<sup>1</sup> Zhiyong Nie,<sup>1</sup> Rui Li,<sup>1</sup> Xin Lu,<sup>1</sup> Hanoh Lee,<sup>1</sup> Michael Smidman,<sup>1,†</sup> Frank Steglich,<sup>1,3</sup> Piers Coleman,<sup>2,‡</sup> and Huiqiu Yuan<sup>1,4,§</sup>

<sup>1</sup>*Center for Correlated Matter and Department of Physics,  
Zhejiang University, Hangzhou 310058, China*

<sup>2</sup>*Department of Physics and Astronomy,  
Rutgers University, Piscataway, New Jersey 08854, USA*

<sup>3</sup>*Max Planck Institute for Chemical Physics of Solids, 01187 Dresden, Germany*

<sup>4</sup>*Collaborative Innovation Center of Advanced Microstructures,  
Nanjing University, Nanjing, 210093, China*

(Dated: December 17, 2019)

The strange metal phases found to develop in a wide range of materials near a quantum critical point (QCP), have posed a long-standing mystery. The frequent association of strange metals with unconventional superconductivity and antiferromagnetic QCPs [1–4] has led to a belief that they are highly entangled quantum states [5]. Ferromagnets, by contrast are regarded as an unlikely setting for strange metals, for they are weakly entangled and their QCPs are often interrupted by competing phases or first order phase transitions [6–8]. Here, we provide compelling evidence that the stoichiometric heavy fermion ferromagnet  $\text{CeRh}_6\text{Ge}_4$  [9, 10] becomes a strange metal at a pressure-induced QCP: specific heat and resistivity measurements demonstrate that the FM transition is continuously suppressed to zero temperature revealing a strange metal phase. We argue that strong magnetic anisotropy plays a key role in this process, injecting entanglement, in the form of triplet resonating valence bonds (tRVBs) into the ordered ferromagnet. We show that the singular transformation from tRVBs into Kondo singlets that occurs at the QCP causes a jump in the Fermi surface volume: a key driver of strange metallic behavior. Our results open up a new direction for research into FM quantum criticality, while also establishing an important new setting for the strange metal problem. Most importantly, strange metallic behavior at a FM quantum critical point suggests that it is quantum entanglement rather than the destruction of antiferromagnetism that is the common driver of the many varied examples of strange metallic behavior.

Quantum materials augmented by strong electronic correlations are promising for applications, but the electronic interactions that empower these materials challenge our understanding. One of the most pressing questions in strongly correlated electronic systems is the origin of the strange metallic behavior which develops at a quantum critical phase transition between a delocalized Fermi liquid (FL), and a localized or partially localized electronic phase. A prime example is the strange metal (SM) phase which develops in the normal state of cuprate superconductors at optimal doping, characterized by a robust linear resistivity and a logarithmic temperature dependence of the specific heat coefficient [2, 3]; similar be-

---

\* These authors contributed equally to this work

† [msmidman@zju.edu.cn](mailto:msmidman@zju.edu.cn)

‡ [coleman@physics.rutgers.edu](mailto:coleman@physics.rutgers.edu)

§ [hqyuan@zju.edu.cn](mailto:hqyuan@zju.edu.cn)

havior is also observed in various quantum critical heavy electron materials. The underlying universality of SM behavior that develops in the vicinity of QCPs is currently a subject of intense theoretical interest. One of the valuable ways of identifying the key ingredients of SM behavior is through experiments that explore new classes of quantum materials.

Kondo lattice systems with periodically arranged atoms hosting localized  $f$ -electrons show a rich variety of properties, due to competition between magnetic interactions among local moments, and their “Kondo” screening by conduction electrons [1]. The small energy scales of these interactions leads to highly tunable ground states, which is ideal for studying SM behavior. In a number of systems, the tuning of the aforementioned competition leads to a continuous suppression of antiferromagnetic (AFM) order at a quantum critical point (QCP)[4]. The outcome when a ferromagnetic (FM) transition is suppressed by a non-thermal tuning parameter is generally different [7]. FM QCPs are often avoided by the occurrence of a first order transition [11], the intersection of AFM phases [12, 13], or a Kondo cluster glass phase [14]. This raises the question of whether AFM correlations are crucial for realizing SM behavior.

Early theoretical studies of itinerant ferromagnets [6, 8] in the framework of Hertz-Millis-Moriya (HMM) theory [15] predicted that quantum phase transitions in these materials are inevitably driven first order by interactions between the critically scattered electron fields, thereby interrupting the development of quantum criticality. However, the recent discovery of a FM QCP in the heavy fermion system  $\text{YbNi}_4\text{P}_2$  tuned by chemical pressure [16], raised the fascinating possibility that the FM QCP in these systems is governed by a different universality class, involving a break-down of Kondo screening [17–19]. The negative pressure required to reach the FM QCP of  $\text{YbNi}_4\text{P}_2$  necessarily involves chemical doping of the stoichiometric compound, which introduces disorder, complicating the theoretical interpretation. Disorder suppresses first order transitions [6], as in the case of  $\text{ZrZn}_2$ , where early experiments suggested the presence of a FM QCP [20], but improved sample quality led to a first order transition [21]. Thus while the experimental data on  $\text{YbNi}_4\text{P}_2$  suggests the existence of FM QCPs, a definitive proof of such behavior in a quantum ferromagnet requires utilizing hydrostatic, rather than chemical pressure. Ce-based heavy fermion ferromagnets, where pressure can cleanly tune the system to a QCP, are ideally suited for such studies.

$\text{CeRh}_6\text{Ge}_4$  is a heavy fermion ferromagnet with a Curie temperature  $T_C = 2.5$  K [10]. The crystal structure (Fig. 1a) consists of triangular lattices of Ce stacked along the  $c$ -axis

[9]. The Ce-Ce separation is much smaller along the  $c$ -axis (3.86 Å) than in the triangular planes (7.15 Å), suggesting a quasi-one-dimensional nature to the magnetism. Under hydrostatic pressure, we find that the FM transition of CeRh<sub>6</sub>Ge<sub>4</sub> is smoothly suppressed to zero temperature, reaching a QCP at  $p_c = 0.8$  GPa.

The temperature dependence of the resistivity  $\rho(T)$  and specific heat (as  $C(T)/T$ ) of single crystalline CeRh<sub>6</sub>Ge<sub>4</sub> both show transition anomalies at around  $T_C \approx 2.5$  K (Figs. 1b and 1c). When magnetic fields are applied within the  $ab$ -plane, the transition becomes a broadened crossover, consistent with FM ordering. The low temperature magnetization (as  $M/H$ ) is shown in Fig 1d. Measurements up to 300 K demonstrate that the magnetic easy direction lies within the  $ab$ -plane (Fig. S1). On cooling, just above  $T_C$ , the in-plane  $M/H$  undergoes a marked enhancement, typical of FM order. For fields along the  $c$ -axis,  $M/H$  abruptly increases at the transition. Magnetization loops below  $T_C$  for in-plane fields show hysteresis characteristic of FM materials (Fig. 1e). At higher fields, there is no hysteresis, and a much less rapid increase of the magnetization with field above  $0.28\mu_B/\text{Ce}$ , which likely corresponds to the ordered moment (Fig. S1).

The zero-field resistivity and specific heat coefficient at various pressures are displayed in Figs. 2a and 2b, respectively (see also Figs. S3 and S4). The evolution of the properties with pressure and the resulting  $T-p$  phase diagram are presented in Figs. 3a and 3b. At  $T_C$  the resistivity crosses over from a  $T$ -linear behavior at high temperature to a  $T^2$  behavior at low temperatures (Fig. S3), where  $C(T)/T$  becomes temperature independent. The FM transition, which is suppressed almost linearly by pressure, cannot be detected anymore beyond  $p_c = 0.8$  GPa. In the paramagnetic (PM) phase above  $p_c$ , the aforementioned low- $T$  FL properties are again observed (Figs. S3 and S4). The temperature at which this FL behavior onsets ( $T_{\text{FL}}$ ) increases almost linearly with pressure (Fig. 3b). Both the value of the low-temperature plateau in  $C(T)/T$  and the  $A$ -coefficient in  $\rho(T) = \rho_0 + AT^2$  show an incipient divergence when approaching  $p_c$  from the FM or PM side (Fig. 3a). On both Fermi-liquid sides of the phase diagram, the Kadowaki-Woods ratio  $A/\gamma^2$  is  $1.49 \times 10^{-6}$  (ambient pressure) and  $1.33 \times 10^{-6} \mu\Omega \text{ cm mol}^2 \text{ K}^2 \text{ mJ}^{-2}$  (1.12 GPa), which are close to the value for a  $4f$ -electron ground state degeneracy  $N = 4$ .

At  $p_c = 0.8$  GPa, the resistivity is strictly linear in temperature over two decades down to at least 40 mK, while  $C(T)/T \propto \log(T^*/T)$  with  $T^* = 2.3$  K ( $T^*$  is a characteristic temperature of the spin fluctuation energies [4]), over more than a decade (Fig. 2c). At

60 mK,  $C(T)/T$  reaches a very large value of  $1.1 \text{ J mol}^{-1}\text{K}^{-2}$ . Between the FM and PM phases, there is a fan-shaped SM region with properties similar to canonical AFM quantum critical systems such as  $\text{CeCu}_{6-x}\text{Au}_x$  [22] and  $\text{YbRh}_2\text{Si}_2$  [23]. The pressure dependences of the  $A$ -coefficient and the Sommerfeld coefficient  $\gamma$  (Fig. 3a) follow the residual resistivity  $\rho_0$ , which also develops a maximum at  $p_c$ , reflecting the presence of strong quantum critical fluctuations (Fig. S3).

At first sight, the strange metal properties of  $\text{CeRh}_6\text{Ge}_4$  might be attributed to itinerant quantum criticality, for aside from the absence of a first order phase transition, HMM theory predicts a logarithmic Sommerfeld coefficient and a  $T$ -linear electron scattering rate, naively equivalent to a  $T$ -linear resistivity [4]. However, the scattering off long-wavelength FM fluctuations does not relax electron currents, and once this effect is included, a  $\rho \sim T^{5/3}$  dependence of the resistivity is expected [4]. A  $T$ -linear resistivity suggests large angle scattering, a feature typical of *local* fluctuations. Moreover, the strength of the logarithmic divergence in the specific heat anomaly, determined by the fit  $C/T \sim \frac{S_0}{T^*} \log(T^*/T)$ , shows that the entropy  $S_0 \sim \frac{1}{10}R \log(2)$  is a large fraction of the local moment entropy, once again suggesting an underlying local mechanism to the quantum criticality. Together with the absence of a first order phase transition, these features provide strong evidence in favor of a local quantum critical point.

In AFM heavy electron metals, the development of a  $T$ -linear resistivity coincides with an abrupt jump in the Fermi surface volume, accompanied by singular charge fluctuations [24–26]. It has been argued that such a jump in the Fermi surface is caused by an abrupt transformation in the pattern of spin entanglement [5], as the Kondo singlets transform into resonating valence bonds (RVBs) in the spin fluid. This leaves us with a puzzle, for the spins in a simple ferromagnet are not entangled, which would imply a *continuous* evolution of the Fermi surface [27]. The unusual aspect of  $\text{CeRh}_6\text{Ge}_4$  is the development of a SM phase at a FM QCP, which shows similar behavior to the non-stoichiometric material  $\text{YbNi}_4\text{P}_{2-x}\text{As}_x$  [16].

Apart from the quasi-1D nature, a common feature of these two materials is an easy-plane anisotropy. In such systems, the magnetic order parameter is no longer conserved and will develop marked zero-point fluctuations, likely responsible for the severely reduced magnetic moment. This can be seen clearly in a two-site example where the magnetization is along the  $x$ -direction. The ordered phase is a product state which can be expanded in terms of

triplets,

$$\left(\frac{|\uparrow_i\rangle + |\downarrow_i\rangle}{\sqrt{2}}\right)\left(\frac{|\uparrow_j\rangle + |\downarrow_j\rangle}{\sqrt{2}}\right) = \frac{|\uparrow_i\uparrow_j\rangle + |\downarrow_i\downarrow_j\rangle}{2} + \frac{1}{\sqrt{2}}\left(\frac{|\uparrow_i\downarrow_j\rangle + |\downarrow_i\uparrow_j\rangle}{\sqrt{2}}\right). \quad (1)$$

An easy-plane anisotropy projects out the equal-spin pairs on the right-hand-side, creating a triplet valence bond. In a lattice, the same effect creates a quantum superposition of triplet pairs, forming a triplet-RVB (tRVB) state, written schematically  $P_G |\text{FM}\rangle = |\text{tRVB}\rangle$ . Hence, an easy-plane anisotropy in FM systems plays the same role as magnetic frustration in AFM systems, injecting a macroscopic entanglement into the ground state. This leads us to hypothesize that the SM behavior at the FM QCP has its origins in the magnetic anisotropy.

To test these ideas, we have studied a simplified Kondo lattice model with nearest neighbor FM couplings with an easy-plane anisotropy of the form  $-J_{xy}^{ij}(S_i^x S_j^x + S_i^y S_j^y) - J_z^{ij} S_i^z S_j^z$  on a tetragonal lattice, consisting of spin chains along the  $c$ -direction with weak inter-chain couplings (see Supplementary Material). When the chains are weakly coupled, our simulations indicate the development of a second order phase transition, while at higher couplings a first order phase transition develops. This feature is in agreement with the current observations of FM QCPs developing in quasi-1D systems. We assume  $J_{xy} > J_z$  which has a dual effect: it converts the model into an easy plane  $x - y$  ferromagnet, and generates triplet resonating valence bonds (tRVB). Also, the anisotropy changes the magnetic dispersion at low momenta from quadratic to linear (see Supplementary Material). By switching on the Kondo screening [26–28] we can then tune the model to the QCP.

Our calculations take advantage of a Schwinger boson representation of the magnetic moments which allows us to treat the magnetic and Kondo-screened parts of the phase diagram, and the QCP that links them together (Fig. 3c). The key feature of this approach, is that the Kondo effect causes the spins to fractionalize into electrons, expanding the Fermi surface while leaving behind positively charged, spinless, Kondo singlets. In the ordered phase, the majority of the moments are aligned, while some form tRVB pairs with their neighbors. In an isotropic ferromagnet, the continuous growth of magnetization away from the QCP, indicates a continuous change in the fraction of Kondo screened moments, or a continuous evolution of the Fermi surface. However, when the moments entangled within tRVB states are abruptly released into the Fermi sea, we find (Supplementary text) that there is a jump in the Fermi surface volume. The resulting QCP is a plasma, in which the Kondo

singlets, the electrons and the RVB bonds are in a state of critical dynamical equilibrium, giving rise to singular spin and charge fluctuations as well as a logarithmic in temperature specific heat coefficient (Supplementary text), in agreement with our experimental results.

Our findings of a pressure-induced QCP in  $\text{CeRh}_6\text{Ge}_4$  demonstrate that a FM system can develop a continuous quantum phase transition in the absence of disorder, a result that at present, can only be understood in the framework of local quantum criticality, where Kondo screening is suppressed to zero at the QCP. The observation of SM behavior at finite temperatures above the QCP with a  $T$ -linear resistivity and a specific heat coefficient that is logarithmically divergent in  $T$ , now expands the scope of this phenomenon to encompass ferromagnets. Central to the SM behavior in a ferromagnet is a small abrupt jump in the Fermi surface volume. An experimental observation of such a jump would be an unambiguous test of Kondo breakdown, as there is no unit-cell doubling at a FM phase transition.

Finally, spin-triplet superconducting pairing states have been proposed in FM heavy-fermion systems, such as  $\text{UGe}_2$  [29] and  $\text{URhGe}$  [30]. While there is no sign of superconductivity in  $\text{CeRh}_6\text{Ge}_4$  down to 40mK, it is very likely that at sufficiently low temperatures, the tRVB states that are already present in the critical regime will migrate into the conduction band as a triplet superconducting condensate.

## Methods

**Crystal growth and characterization.** Needle-like shaped single crystals of  $\text{CeRh}_6\text{Ge}_4$  were grown using a Bi flux [9]. The elements were combined in a molar ratio of Ce:Rh:Ge:Bi of 1:6:4:150, and sealed in an evacuated quartz tube. The tube was heated and held at  $1100^\circ\text{C}$  for 10 hours, before being cooled at  $3^\circ\text{C}/\text{hour}$  to  $500^\circ\text{C}$ . The tube was then removed, and centrifuged to remove the excess Bi. The orientation of the crystals was determined using single crystal x-ray diffraction, and the chemical composition was confirmed using energy dispersive x-ray spectroscopy. The samples measured under pressure had typical values of  $\rho_0 \approx 1.6 \mu\Omega \text{ cm}$  and  $RRR = \rho(300 \text{ K})/\rho(0.3 \text{ K}) \approx 45$  (Fig. S2).

**Physical property measurements.** Magnetization measurements were performed using a Quantum Design Magnetic Property Measurement System (MPMS). The heat capacity at ambient pressure was measured down to 0.4 K, in applied magnetic fields up to 14 T, using a Quantum Design Physical Property Measurement (PPMS) system with a  $^3\text{He}$  insert, utilizing the standard relaxation method. Specific heat experiments under pressure were carried out using a CuBe piston-cylinder-type pressure cell [31]. The sample and a piece of lead as pressure gauge were put in a teflon capsule together with Fluinert serving as liquid pressure transmitting medium. The capsule was then mounted inside the pressure cell. The heat capacity of the whole assembly was determined by a compensated heat-pulse method in a dilution refrigerator (Oxford Instruments) down to temperatures of 60 mK. To obtain the heat capacity of the sample the addenda has been recorded in a separate measurement run and subtracted for each pressure from the data obtained of the whole setup including the sample. The pressure inside the cell was determined by the pressure-induced shift of the superconducting transition temperature of the piece of lead measured in a Quantum Design MPMS. The magnetic field was removed in an oscillating fashion to reduce the remanent field ( $< 3 \text{ Oe}$ ) of the superconducting magnet. The remaining effect on the superconducting transition temperature was compensated for by determining the shift of the superconducting transition of the lead inside the pressure cell with respect to a reference piece fixed to the outside. Electrical transport and ac calorimetry measurements under pressure were carried out in a piston-cylinder clamp-type cell with Daphne oil 7373 as a pressure transmitting medium. The pressure was also determined from the superconducting transition of Pb. The resistivity was measured using the four contact configuration between 0.05 K and 300 K. The measurements between 1.9 K and 0.4 K were performed in a  $^3\text{He}$  refrigerator.



**Data availability** All the data supporting the findings are available from the corresponding author upon reasonable request.

**Acknowledgments** We would like to thank Cornelius Krellner and Manuel Brando for fruitful discussions, Guanghan Cao and Zhicheng Wang for assisting with  $^3\text{He}$ -SQUID measurements, and Xiaoyan Xiao for assistance with single crystal x-ray diffraction. This work was supported by the National Key R&D Program of China (No. 2017YFA0303100, No. 2016YFA0300202), the National Natural Science Foundation of China (No. U1632275), the Science Challenge Project of China (No. TZ2016004) and the National Science Foundation of the United States of America, grant DMR-1830707.

**Additional information** Correspondence and requests for materials should be addressed to H. Q. Yuan (hqyuan@zju.edu.cn), P. Coleman (coleman@physics.rutgers.edu) or M. Smidman (msmidman@zju.edu.cn).

**Author contributions** The project was conceived by H. Y.. The crystals were grown by Y. Z. and H. L., and measurements were performed by B. S., Y. Z., M. N., R. B., A. W., Y. C., Z. N., R. L., and X. L.. The experimental data were analyzed by B. S., Y. Z., M. N., H. L., M. S., F. S. and H. Y.. Theoretical calculations were performed by Y. K. and P. C.. The manuscript were written by Y. K., M. S., F. S., P. C., and H. Y. All authors participated in discussions.

**Competing financial interests** The authors declare no competing financial interests.

- 
- [1] Gegenwart, P., Si, Q. & Steglich, F. Quantum criticality in heavy-fermion metals. *Nature Phys.* **4**, 186–197 (2008). URL <http://dx.doi.org/10.1038/nphys892>.
  - [2] Daou, R. *et al.* Linear temperature dependence of resistivity and change in the Fermi surface at the pseudogap critical point of a high- $T_c$  superconductor. *Nature Physics* **5**, 31 (2008). URL <https://doi.org/10.1038/nphys1109>.
  - [3] Legros, A. *et al.* Universal  $T$ -linear resistivity and Planckian dissipation in overdoped cuprates.

- Nature Physics* **15**, 142–147 (2019). URL <https://doi.org/10.1038/s41567-018-0334-2>.
- [4] Stewart, G. R. Non-Fermi-liquid behavior in  $d$ - and  $f$ -electron metals. *Rev. Mod. Phys.* **73**, 797–855 (2001). URL <https://link.aps.org/doi/10.1103/RevModPhys.73.797>.
- [5] Senthil, T., Vojta, M. & Sachdev, S. Weak magnetism and non-Fermi liquids near heavy-fermion critical points. *Phys. Rev. B* **69**, 035111 (2004). URL <https://link.aps.org/doi/10.1103/PhysRevB.69.035111>.
- [6] Belitz, D., Kirkpatrick, T. R. & Vojta, T. First order transitions and multicritical points in weak itinerant ferromagnets. *Phys. Rev. Lett.* **82**, 4707–4710 (1999). URL <https://link.aps.org/doi/10.1103/PhysRevLett.82.4707>.
- [7] Brando, M., Belitz, D., Grosche, F. M. & Kirkpatrick, T. R. Metallic quantum ferromagnets. *Rev. Mod. Phys.* **88**, 1–71 (2016). URL <http://link.aps.org/doi/10.1103/RevModPhys.88.025006>.
- [8] Chubukov, A. V., Pépin, C. & Rech, J. Instability of the quantum-critical point of itinerant ferromagnets. *Phys. Rev. Lett.* **92**, 147003 (2004). URL <https://link.aps.org/doi/10.1103/PhysRevLett.92.147003>.
- [9] Vosswinkel, D., Niehaus, O., Rodewald, U. C. & Pöttgen, R. Bismuth flux growth of  $\text{CeRh}_6\text{Ge}_4$  and  $\text{CeRh}_2\text{Ge}_2$  single crystals. *Zeitschrift für Naturforschung B* **67**, 1241–1247 (2012). URL <https://doi.org/10.5560/znb.2012-0265>.
- [10] Matsuoka, E. *et al.* Ferromagnetic transition at 2.5K in the hexagonal Kondo-lattice compound  $\text{CeRh}_6\text{Ge}_4$ . *J. Phys. Soc. Jpn.* **84**, 073704 (2015). URL <http://dx.doi.org/10.7566/JPSJ.84.073704>.
- [11] Pfeleiderer, C., McMullan, G. J., Julian, S. R. & Lonzarich, G. G. Magnetic quantum phase transition in  $\text{MnSi}$  under hydrostatic pressure. *Phys. Rev. B* **55**, 8330 (1997). URL <https://link.aps.org/doi/10.1103/PhysRevB.55.8330>.
- [12] Süllow, S., Aronson, M. C., Rainford, B. D. & Haen, P. Doniach phase diagram, revisited: From ferromagnet to Fermi liquid in pressurized  $\text{CeRu}_2\text{Ge}_2$ . *Phys. Rev. Lett.* **82**, 2963–2966 (1999). URL <https://link.aps.org/doi/10.1103/PhysRevLett.82.2963>.
- [13] Brando, M. *et al.* Logarithmic Fermi-liquid breakdown in  $\text{NbFe}_2$ . *Phys. Rev. Lett.* **101**, 026401 (2008). URL <https://link.aps.org/doi/10.1103/PhysRevLett.101.026401>.
- [14] Westerkamp, T. *et al.* Kondo-cluster-glass state near a ferromagnetic quantum phase transition. *Phys. Rev. Lett.* **102**, 026404 (2009). URL <http://link.aps.org/doi/10.1103/>

- [PhysRevLett.102.206404](#).
- [15] Sachdev, S. *Quantum Phase Transitions* (Cambridge University Press, 2011), 2 edn. URL <https://doi.org/10.1017/CB09780511973765>.
- [16] Steppke, A. *et al.* Ferromagnetic quantum critical point in the heavy-fermion metal  $\text{YbNi}_4(\text{P}_{1-x}\text{As}_x)_2$ . *Science* **339**, 933–936 (2013). URL <https://doi.org/10.1126/science.1230583>.
- [17] Custers, J. *et al.* The break-up of heavy electrons at a quantum critical point. *Nature* **424**, 524–527 (2003). URL <http://dx.doi.org/10.1038/nature01774>.
- [18] Schröder, A. *et al.* Onset of antiferromagnetism in heavy-fermion metals. *Nature* **407**, 351–355 (2000). URL <http://dx.doi.org/10.1038/35030039>.
- [19] Yamamoto, S. J. & Si, Q. Metallic ferromagnetism in the Kondo lattice. *Proceedings of the National Academy of Sciences* **107**, 15704–15707 (2010). URL <https://www.pnas.org/content/107/36/15704>.
- [20] Smith, T. F., Mydosh, J. A. & Wohlfarth, E. P. Destruction of ferromagnetism in  $\text{ZrZn}_2$  at high pressure. *Phys. Rev. Lett.* **27**, 1732–1735 (1971). URL <https://link.aps.org/doi/10.1103/PhysRevLett.27.1732>.
- [21] Uhlarz, M., Pfleiderer, C. & Hayden, S. M. Quantum phase transitions in the itinerant ferromagnet  $\text{ZrZn}_2$ . *Phys. Rev. Lett.* **93**, 256404 (2004). URL <https://link.aps.org/doi/10.1103/PhysRevLett.93.256404>.
- [22] Löhneysen, H. v. *et al.* Non-Fermi-liquid behavior in a heavy-fermion alloy at a magnetic instability. *Phys. Rev. Lett.* **72**, 3262–3265 (1994). URL <https://link.aps.org/doi/10.1103/PhysRevLett.72.3262>.
- [23] Trovarelli, O. *et al.*  $\text{YbRh}_2\text{Si}_2$ : Pronounced non-Fermi-liquid effects above a low-lying magnetic phase transition. *Phys. Rev. Lett.* **85**, 626–629 (2000). URL <https://doi.org/10.1103/PhysRevLett.85.626>.
- [24] Paschen, S. *et al.* Hall-effect evolution across a heavy-fermion quantum critical point. *Nature* **432**, 881–885 (2004). URL <http://dx.doi.org/nature10.1038/03129>.
- [25] Shishido, H., Settai, R., Harima, H. & Ōnuki, Y. A drastic change of the Fermi surface at a critical pressure in  $\text{CeRhIn}_5$ : dHvA study under pressure. *J. Phys. Soc. Jpn.* **74**, 1103–1106 (2005). URL <https://doi.org/10.1143/JPSJ.74.1103>.
- [26] Komijani, Y. & Coleman, P. Emergent critical charge fluctuations at the Kondo breakdown

- of heavy fermions. *Phys. Rev. Lett.* **122**, 217001 (2019). URL <https://link.aps.org/doi/10.1103/PhysRevLett.122.217001>.
- [27] Komijani, Y. & Coleman, P. Model for a ferromagnetic quantum critical point in a 1D Kondo lattice. *Phys. Rev. Lett.* **120**, 157206 (2018). URL <https://link.aps.org/doi/10.1103/PhysRevLett.120.157206>.
- [28] Wang, J., Chang, Y.-Y., Mou, C.-Y., Kirchner, S. & Chung, C.-H. Quantum phase transition in a two-dimensional Kondo-Heisenberg model: a Schwinger-boson large-N approach. *ArXiv:1901.10411* (2019).
- [29] Saxena, S. S. *et al.* Superconductivity on the border of itinerant-electron ferromagnetism in UGe<sub>2</sub>. *Nature* **406**, 587–592 (2000). URL <https://doi.org/10.1038/35020500>.
- [30] Lévy, F., Sheikin, I., Grenier, B. & Huxley, A. D. Magnetic field-induced superconductivity in the ferromagnet URhGe. *Science* **309**, 1343 (2005). URL <http://science.sciencemag.org/content/309/5739/1343.abstract>.
- [31] Nicklas, M. & Avella, A. In Mancini, F. (ed.) *Strongly Correlated Systems - Experimental Techniques*, Springer Series in Solid-State Sciences.

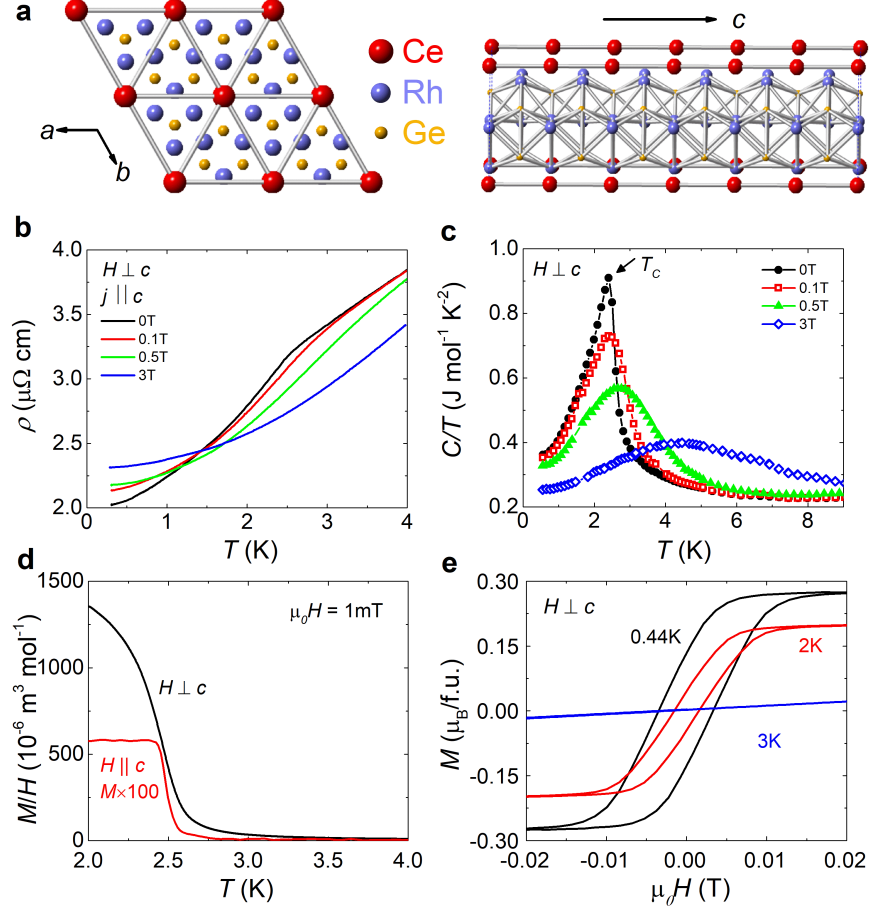


FIG. 1. Crystal structure and physical properties of  $\text{CeRh}_6\text{Ge}_4$  at ambient pressure.

**a**, Crystal structure of  $\text{CeRh}_6\text{Ge}_4$ , where the red, blue and yellow atoms denote Ce, Rh, and Ge respectively. Left panel shows the structure perpendicular to the  $ab$ -plane, where the Ce atoms have a hexagonal arrangement, while the right side displays perpendicular to the chain direction ( $c$ -axis). The **b**, resistivity  $\rho(T)$ , and **c**, specific heat as  $C/T$  vs  $T$  of  $\text{CeRh}_6\text{Ge}_4$  are also displayed, in both zero-field and various fields applied within the  $ab$  plane. **d**, Temperature dependence of the magnetization of  $\text{CeRh}_6\text{Ge}_4$  as  $M/H$  in a field of 1 mT applied both along the  $c$  axis and in the  $ab$  plane. **e**, Low field magnetization loops for fields within the  $ab$ -plane at three temperatures. Below  $T_C$ , these exhibit hysteresis loops typical of FM order, while at 3 K no hysteresis is observed.

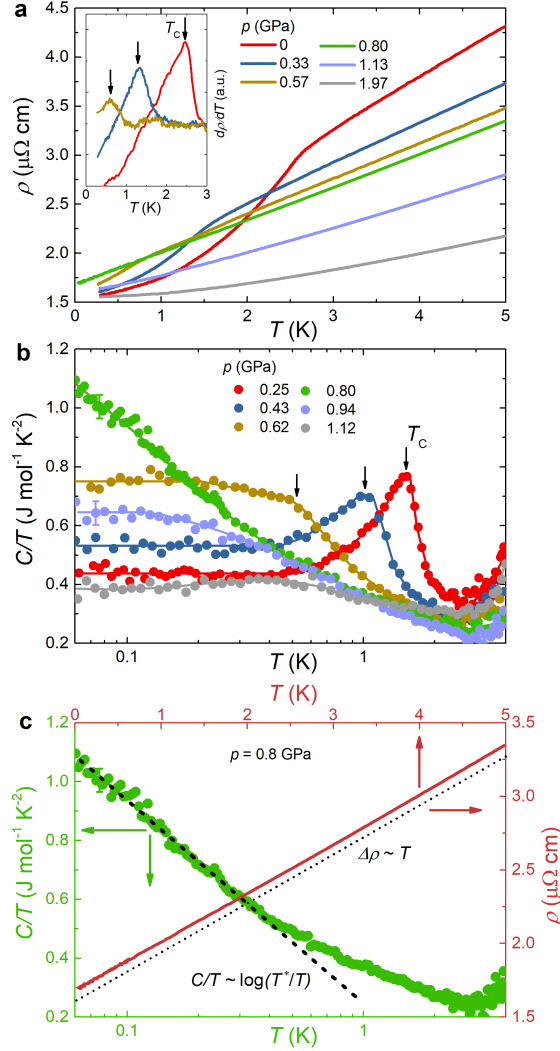


FIG. 2. **Pressure evolution of ferromagnetism in  $\text{CeRh}_6\text{Ge}_4$  and strange metallic behavior at the quantum critical point.** **a**, Resistivity of  $\text{CeRh}_6\text{Ge}_4$  under various hydrostatic pressures. The FM transition is suppressed by pressure, and is no longer observed at  $p_c = 0.8$  GPa (green line). The inset shows the derivative of  $\rho(T)$  at lower pressures, where the peak position corresponds to  $T_C$ . **b**, Specific heat of  $\text{CeRh}_6\text{Ge}_4$  under hydrostatic pressures, where the bulk FM transition is suppressed with pressure, as indicated by the vertical arrows showing the position of  $T_C$ . For clarity, not all the data points are displayed. The error bars shown are representative of the scattering of the data at low temperature. A crossover to FL behavior at low temperatures can be observed either side of  $p_c$ , where  $C(T)/T$  flattens. **c**,  $\rho(T)$  and  $C(T)/T$  at  $p_c = 0.8$  GPa.  $\rho(T)$  exhibits linear behavior extending from 5 K, down to at least 40 mK (dotted line), while  $C(T)/T$  continues to increase with decreasing temperature, exhibiting a  $\sim \log(T^*/T)$  dependence (dashed line).

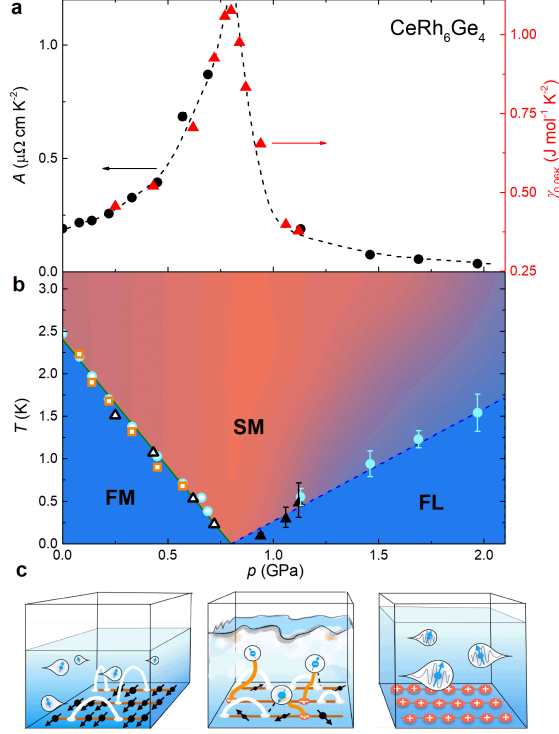


FIG. 3. **Phase diagram of  $\text{CeRh}_6\text{Ge}_4$  under pressure.** **a**, Pressure dependence of the  $A$ -coefficient of the  $T^2$  term from the resistivity and Sommerfeld coefficient  $\gamma$  (as  $C/T$  at 60 mK), which show a pronounced maximum near the QCP. **b**, Temperature-pressure phase diagram of  $\text{CeRh}_6\text{Ge}_4$ , where the open circles, triangles and squares denote  $T_C$  derived from the resistivity, specific heat (dc method), and ac heat capacity (Fig. S5), respectively. The corresponding solid symbols mark  $T_{\text{FL}}$ , the temperature below which FL behavior occurs. The FM transition is suppressed by pressure until the system reaches a QCP at  $p_c \approx 0.8$  GPa. Below  $T_C$ , and at higher pressures below  $T_{\text{FL}}$ , FL ground states develop. These phases (shaded blue) are separated by a fan-shaped region of non-Fermi liquid behavior, where around  $p_c$  there is a SM phase (shaded red) showing a linear in temperature resistivity and logarithmic  $C/T$  vs  $T$ . **c**, The schematic representation of different phases. In the ordered phase (left), most of the spins are ordered in the plane, whereas some have RVB bonds. The Fermi surface is small, as represented by the volume of the conduction sea. In the PM FL phase (right), all the spins are ‘ionized’ to form heavy-electrons that expand the Fermi sea. A background of positively charged singlets are left behind. At the QCP (center), the system is in dynamical critical equilibrium, where the moments are fluctuating and the Kondo screening by the conduction electron competes with RVBs for the entanglement. In this region, critical fluctuations strongly scatter the conduction electrons.